Environmental Science Nano

Interaction of Supported Phospholipid Bilayers with Diamond Nanoparticles Non-Covalently Functionalized with a Cationic Polyelectrolyte

Journal:	*Environmental Science: Nano*
Manuscript ID	EN-ART-05-2023-000349.R1
Article Type:	Paper

Environmental Significance Statement

As engineered nanoparticles find increasing use in applications from agriculture to batteries to biomedical purposes, they also find increasing release into the environment. It is important to understand the mechanistic interactions of nanoparticles with biological interfaces to predict toxicity and thereby engineer more sustainable and safer nanomaterials. In this study, we demonstrate that not only do positively charged polyallylamine hydrochloride-wrapped diamond nanoparticles attach to negatively charged phospholipid bilayers via electrostatics, but they go further and extract lipid from the bilayers via contact ion pairing. Our study contributes to determining structure-property-interaction relationships between NPs and model biological interfaces for assessing nanoparticle toxicity and guiding future nanoparticle design.

ARTICLE

Interaction of Supported Phospholipid Bilayers with Diamond Nanoparticles Non-Covalently Functionalized with a Cationic Polyelectrolyte

Received 00th January 20xx,
Accepted 00th January 20xx

DOI: 10.1039/x0xx00000x

Thomas R. Kuech,[a,#] Nasim Ganji,[a,#] Caroline Anastasia,[b] Marco D. Torelli,[c] Eric. S. Melby,[a] Arielle C. Mensch,[c,d] Emily R. Caudill,[c] Ralf Zimmermann,[d] Robert J. Hamers,[c*] Joel A. Pedersen[a,c,e,f]

We use diamond nanoparticles (DNPs) wrapped in the cationic polyelectrolyte poly(allylamine) hydrochloride (PAH) and bilayers composed of either pure DOPC or a mixture of DOPC/DOPG to investigate the influence of membrane phospholipid composition and net surface charge on nanoparticle-membrane interactions and the extent of nanoparticle adhesion to supported phospholipid bilayers. Our results show that in all cases electrostatic attractions between the negatively charged bilayer and cationic PAH-DNP were responsible for the initial attachment of particles, and the lateral electrostatic repulsion between adsorbed particles on the bilayer surface determined the final extent of PAH-DNP attachment. Upon attachment, NPs attract lipids by the contact ion pairing between the ammonium groups on PAH and phosphate and glycerol groups on the lipids and acquire a lipid corona. Lipid corona formation on the PAH-DNP reduces the effective charge density of the particle and is in fact a key factor determining the final extent of NP attachment to the bilayer. Incorporation of DOPG to the bilayer leads to a decrease in efficiency and final extent of attachment compared to DOPC alone. The reduction in PAH-DNP attachment in the presence of DOPG is attributed to the adsorption of free PAH in equilibrium with bound PAH in the nanoparticle solution, thus reducing electrostatic attraction between PAH-DNPs and SLBs. This leads to an increase in hydrogen bonding interactions between lipid headgroups that limits extraction of phospholipids from the bilayer by PAH-DNP, lessening the reduction in interparticle repulsion achieved by acquisition of a lipid corona. Our results indicate that the inclusion of charged phospholipids in SLBs changes bilayer rigidity and stability and hinders the attachment of PAH-DNPs by preventing lipid extraction from the bilayer.

Environmental Significance

As engineered nanoparticles find increasing use in applications from agriculture to batteries to biomedical purposes, they also find increasing release into the environment. It is important to understand the mechanistic interactions of nanoparticles with biological interfaces to predict toxicity and thereby engineer more sustainable and safer nanomaterials. In this study, we demonstrate that not only do positively charged PAH-wrapped diamond nanoparticles attach to negatively charged phospholipid bilayers via electrostatics, but

[a.] *Environmental Chemistry and Technology Program, University of Wisconsin, Madison, WI 53706, USA*
[b.] *Department of Chemistry, Johns Hopkins University, Baltimore, MD 21218, USA*
[c.] *Department of Chemistry, University of Wisconsin, Madison, WI 53706, USA*
[d.] *Leibniz Institute of Polymer Research Dresden, Dresden, Germany*
[e.] *Department of Environmental Health and Engineering, Johns Hopkins University, Baltimore, MD 21218, USA*
[f.] *Deceased*
**Corresponding author*
#These authors contributed equally to this work
Electronic Supplementary Information (ESI) available: See DOI: 10.1039/x0xx00000x

they go further and extract lipid from the bilayers via contact ion pairing. Our study contributes to determining structure-property-interaction relationships between NPs and model biological interfaces for assessing nanoparticle toxicity and guiding future nanoparticle design.

Introduction

Rising production and use of engineered nanoparticles (NPs) in diverse applications has undoubtedly led to the release of these materials into the environment.[1,2] As NPs enter the environment, evaluating their interaction with biological systems is a key aspect toward understanding their impact on environmental health and safety.[3–6] Nanotoxicity studies have shown that NPs can interact with cell membranes and induce cytotoxicity.[1,7] Although the pathways for cytotoxicity are diverse and depend on nanoparticle physicochemical properties and cell type,[8] recent studies have provided evidence that direct contact between nanomaterials and the cell membrane is necessary for membrane damage or cell inactivation; it may in fact be a primary mechanism for engineered nanomaterial (ENM)-induced cytotoxicity.[9–13] The interfacial and biological interactions between nanoparticles and cell surfaces that modulate this process can be examined using model cell membranes.[14–26]

Model membranes, in the form of supported lipid bilayers, have been used extensively to examine the adhesion of, and subsequent disruption by, carbon nanotubes,[27,28] quantum dots,[29–31] carbon dots,[32] and gold,[33–35] silica,[36,37] and polystyrene[38–40] nanoparticles. Two main advantages of model membranes are that: (1) the lipid composition can be precisely controlled, thereby mimicking some of the most relevant physicochemical features of the real cell membrane,[32] and (2) the membrane organization and disruption can be characterized directly using a range of surface-sensitive techniques that are not easily applicable on living cells.[21] These simplified structures enable controlled and systematic study of the chemical components that serve important roles in the function of the cell membrane.[41,42]

In the context of nanoparticle-membrane interactions, Leroueil et al. have shown that both organic and inorganic cationic nanoparticles can induce defects in SLBs and that the physical disruption of lipid membranes and formation of holes and/or thinned regions is a common mechanism of interaction between cationic nanoparticles and lipids.[1,36] Earlier work comparing the interaction of cationic and anionic quantum dots (QDs) with SLBs showed the adhesion of QDs to phospholipid bilayers is driven by nonspecific electrostatic interactions, and depends on bilayer composition (e.g., net surface charge) and the ionic strength of the surrounding medium.[29] Similar works using giant unilamellar vesicles,[43] liposomes,[44] lipid monolayers[21], and sulfolipid-containing bilayers[32] as a model membrane indicated that nanoparticle adhesion to lipid-based model membranes depends on nanoparticle charge, and cationic nanoparticles have higher affinity compared to anionic nanoparticles for membrane adsorption and disruption.[45]

Poly(allylamine hydrochloride) (PAH) is a polycation, commonly used for polyelectrolyte-wrapping of colloidal nanoparticles.[33,46–48] Because an excess amount of polyelectrolyte is usually employed during the surface modification process, free or unbound ligand can remain in nanoparticle solutions even after purification[49] and affect NPs intrinsic toxicity.[50,51] Although the adsorption of PAH to lipid bilayers has been found to be reversible and nondisruptive,[52] PAH-NPs solutions have been shown to bind irreversibly to supported lipid bilayers[33] and exhibit toxicity to bacteria[49,53] and simple multicellular organisms.[54,55] Mechanistic insight into the influence of excess ligand in NP solutions on the interaction of non-covalently functionalized NPs with cell membranes are needed to understand and control interactions at nano-bio interfaces and aid in the design of environmentally and biologically compatible polycation-wrapped NPs.

The objectives of this study were to examine the effects of ionic strength and bilayer composition on the interaction of non-covalently PAH-functionalized DNPs with SLBs and to determine the influence of free PAH polymer, in equilibrium with bound PAH in nanoparticle solutions, on the efficiency and extent of PAH-DNP attachment to SLBs. To accomplish these objectives, we employed quartz crystal microbalance with dissipation monitoring (QCM-D) and atomic force microscopy (AFM) to examine the interactions between diamond nanoparticles (DNPs) wrapped in PAH (~190 repeat units), and supported lipid bilayers. Bilayers were composed of a zwitterionic phospholipid and 0 to 20% of an anionic phospholipid. Experiments were conducted over a range of ionic strength values (I = 0.006–0.106 M) to investigate the influence of electrostatic interactions on the extent of particles attachment to model membranes and lipid extraction from the bilayers.

Materials and methods

Materials. We purchased 1,2-dioleoyl-*sn*-glycero-3-phosphocholine (DOPC), 1,2-dioleoyl-*sn*-glycero-3-phospho-(1'-*rac*-glycerol) (DOPG) from Avanti Polar Lipids Inc. (Alabaster, AL). Poly(allylamine hydrochloride) (PAH, 15 kDa) was procured from Sigma Aldrich (Milwaukee, WI). The chemical structure of lipids and PAH polymer are presented in Table S1. Diamond nanoparticles (Monocrystalline Synthetic Diamond, MSY 0-0.03 µm) were obtained from Microdiamant (Lengwil, Switzerland). Tris(hydroxymethyl) aminomethane (Tris, 99.8%), NaCl (99.0%), HNO_3 (70.0%), H_2SO_4 (98.0%), H_2O_2 (30.0%), NH_4OH (29%), and concentrated HCl were from Fisher Scientific (Milwaukee, WI). Ultrapure water (18.2 MΩ·cm resistivity) was obtained from a Barnstead GenPure Pro UV purification system (Thermo Scientific). Solutions were prepared in 0.01 M Tris buffer solution; pH was adjusted to 7.4 with 2 M HCl and ionic strength was adjusted to the indicated values using NaCl. All materials were used as received unless otherwise noted.

Functionalization and Characterization of Diamond Nanoparticles. We wrapped DNPs with PAH following a previously described procedure.[56] As-received DNPs were oxidized under reflux with a mixture of sulfuric acid and nitric acid (3:1 (v/v) H_2SO_4:HNO_3) for 3 days. After oxidation, particles were diluted (10×) in ultrapure water and sedimented by centrifugation (5 min, 4696*g*). The supernatant was removed, and the pellet containing DNPs was resuspended in ultrapure water. The centrifugation and resuspension steps were repeated twice, and the remaining pellet was resuspended in 3:1 (v/v) H_2SO_4:HNO_3 and refluxed for another 3 days. The subsequent DNP suspension was diluted, centrifuged (5 min, 4696*g*), and resuspended repeatedly until the pH was neutral and the particles did not sediment. The dispersed particles were wrapped with PAH by mixing particles with polymer solution (10 mg·mL^{-1} in 0.001 M NaCl) at 1:1 (v/v) overnight. Excess polymer was removed by dialysis (Spectrum Laboratories, nominal MWCO 25 kDa) against 12 L ultrapure water.

We determined nanoparticle hydrodynamic diameters (d_h) and ζ-potentials by dynamic light scattering and laser Doppler electrophoresis microelectrophoresis (Malvern ZetaSizer, Worcestershire, UK). Nanoparticle stock solutions were diluted with 0.001 to 0.1 M NaCl buffered to pH 7.4 (0.01 M Tris), and measurements were made at 25 °C. Number-averaged hydrodynamic diameters were calculated from the particle diffusivities using Stokes−Einstein equation and Mie theory.[57] ζ-potentials were estimated from the electrophoretic mobility using the Smoluchowski approximation.[58] The number-averaged hydrodynamic diameters and a ζ-potentials reported are averages of six independent measurements.

Preparation and Characterization of Lipid Vesicles. We prepared small unilamellar vesicles (SUVs) following a published protocol.[34] In brief, a 1 mg·mL^{-1} solution of the desired ratio of DOPC and DOPG was prepared in chloroform. The solvent was removed under a stream of nitrogen gas, followed by drying under vacuum overnight. The dried film was rehydrated in 0.01 M NaCl buffered to pH 7.4 with 0.01 M Tris, sonicated for 30 min in a bath sonicator and subjected to three cycles of freeze-thawing (5 min freeze in liquid nitrogen followed by 5 minutes in a bath sonicator). Aliquots (1 mL) of this suspension were extruded 11 times through a 0.05 µm polycarbonate membrane using an extruder kit (Avanti, 610000) to produce unilamellar vesicles with a narrow size distribution. The vesicle suspension was diluted to 0.125 mg·mL^{-1} total lipid concentration, stored at 4 °C and used within 10 days of preparation. We determined vesicle hydrodynamic diameters and ζ-potentials by dynamic light scattering and laser Doppler electrophoresis as described above for nanoparticles.

Quartz Crystal Microbalance with Dissipation Monitoring (QCM-D). We examined the interaction of PAH-wrapped DNPs with supported lipid bilayers formed on SiO_2-coated quartz crystal sensors (QSX 303, Biolin Scientific) mounted in temperature-controlled liquid flow cells (QFM 401) using a Q-Sense E4 instrument (Biolin Scientific). The QCM-D technique measures changes in both resonance frequency (Δ*f*) and energy dissipation (Δ*D*) of a coated piezoelectric quartz crystal upon interaction with an analyte. Changes in frequency are proportional to the mass of materials adsorbed on the sensor surface, which includes the mass of analyte and dynamically coupled solvent. The dissipation factor represents the fractional energy loss during one oscillation cycle and are related to the viscoelastic properties of laterally homogeneous adlayer or to the rigidity of particle-surface contact zone for laterally heterogeneous films composed of discrete nanoscale objects.[29,59,60] For acoustically rigid films (e.g., SLBs) with low dissipation, $\Delta D_n/(-\Delta f_n/n) << 4 \times 10^{-7}$ Hz^{-1}, the acoustic surface mass density ($\Gamma_{QCM\text{-}D}$) is related to the changes in resonance frequency (Δf_n) using the Sauerbrey equation:[61,62]

$$_{QCM-D} = -\frac{C}{n}\Delta f_n \qquad (1)$$

where C is the mass sensitivity constant which depends on the fundamental frequency, f_1, and crystal properties (C = 17.7 ng·cm^{-2}·Hz^{-1} for the 4.96 MHz crystal used here), and n is the harmonic number. For nonrigid films with large dissipation (e.g., vesicles at critical vesicle coverage), both the frequency and dissipation responses display harmonic dependencies. For such films, the Voigt-Kelvin viscoelastic model was used to quantify the mass associated with the sensor surface. This model extends QCM-D responses to include the effective viscoelastic properties that cause overtone dependencies. [63,64]

Supported phospholipid bilayers were formed on SiO_2-coated quartz crystal sensors from SUVs composed of DOPC or binary mixtures of DOPC and DOPG (9:1 and 8:2 mass ratios) via the vesicle fusion method.[65,66] Cleaned sensors were equilibrated in a solution mixture of 0.1 M NaCl and 0.005 M $CaCl_2$. Details on sensor cleaning procedure are provided in Text S1. Vesicles (0.125 mg·mL^{-1}) in a solution of the same composition were flowed over the sensors until the critical surface coverage of adsorbed vesicles was attained (indicated by maximum changes in the frequency and dissipation responses)[60] and thereafter, vesicles fused and ruptured to form a bilayer. Once the frequency and dissipation values stabilized, the bilayers were rinsed sequentially with the vesicle-free solution described above and 0.1 M NaCl to remove any loosely adhering vesicles.

After formation, supported lipid bilayers were equilibrated with 0.001 to 0.1 M NaCl (pH 7.4 with 0.01 M Tris). PAH-wrapped diamond nanoparticle suspensions (12.8 nM) in the same solution were then flowed over the supported lipid bilayers and particle attachment was monitored for at least 20 min or until the frequency response attained a plateau (df_5/dt < 0.05 Hz·min^{-1}). After 20 min or stabilization, bilayers were rinsed with nanoparticle-free solution to examine the reversibility of attachment.

Initial attachment rates (r_d) were defined as the first derivative of the change in acoustic surface mass density with respect to time over the first 30 s of attachment. The attachment efficiency (α_d) is calculated from attachment rates (r_d):[67,68]

$$\alpha_d = \frac{r_{d,bilayer}}{r_{d,fav}} = \frac{\left(d\Gamma_{QCM-D}/dt\right)_{bilayer}}{\left(d\Gamma_{QCM-D}/dt\right)_{fav}} \qquad (2)$$

where $d\Gamma_{QCM\text{-}D}/dt$ is the change in adsorbed surface mass density per unit time and the subscript "fav" represents the change in adsorbed surface mass density under favorable adsorption conditions where the nanoparticles carry the opposite charge to the surface of the QCM-D sensors and hence there is no energy barrier to adsorption. In this study, we approximated favorable adsorption conditions for the positively charged PAH-DNPs using the strongly negatively charged SiO_2 surface[56,69] and determined initial rates of attachment to SiO_2 under the same solution conditions used for the bilayers. Assuming that PAH-DNP attachment to the silica surface is largely irreversible (the changes in resonance frequency upon rinsing < 1 Hz) and multilayer adsorption does not take place (PAH-DNP attachment to the SiO_2 substrates does not exceed the estimated jamming limit), the total dry surface mass density of PAH-DNP on the sensor surface can be expressed as:[70]

$$\Gamma = \Gamma^*\left(1 - e^{-\left(\frac{k_a m_s}{\Gamma^*}\right)t}\right) \qquad (3)$$

Where Γ^* is the maximum surface density of PAH-DNP that can cover the silica surface (not to exceed the jamming limit), m_s is the bulk solution concentration of NP, and k_a is the adsorption rate constant and can be calculated as:

$$k_a = D_c^{2/3} Q^{1/3} n \qquad (4)$$

where D_c is the diffusivity, Q is the total volumetric flow, and n is a geometrical constant, which is equal to 4.44 × 10^3 m$^{-4/3}$ for the QCMD chamber (E1, Biolin Scientific).[71] We approximated PAH-DNP molar mass on the basis of XPS quantitative analysis of the surface structure of covalently PAH-functionalized DNPs by Zhang et al. yielding an average surface coverage of 1.3 ± 0.06 PAH strands per nm^2 of the DNPs.[72]

Control experiments were conducted in the absence of SLBs to assess the attachment of PAH-DNPs to strongly negatively charged SiO_2-coated sensors and establish a baseline for attachment under favorable conditions (absence of an energy barrier). PAH (50 mg·L^{-1}) adsorption to bare SiO_2 substrates and to SLBs in the absence of DNPs was also examined. The choice of 50 mg·L^{-1} PAH was based on a prior analysis of the amount of free PAH polymer present in PAH-AuNP suspensions purified through diafiltration.[49] In a subset of experiments, the bilayers were first exposed to 50 mg·L^{-1} PAH polymer prior to the introduction of PAH-DNPs to examine the influence of adsorbed polymer on nanoparticles attachment to the bilayers. The flow rate

(100 μL·min^{-1}) and temperature (25 °C) were held constant throughout all the experiments. The odd harmonics (n = 3−11) were measured simultaneously. Data from odd harmonics 3 through 11 were equivalent;[73] we report data from the fifth harmonic (~25 MHz). Representative frequency and dissipation traces for 9:1 DOPC:DOPG SLBs formation and PAH-DNPs attachment are illustrated in Figure S1. All bilayers had $-\Delta f_5/5 = 24.5 \pm 1.5$ Hz and $\Delta D_5 < 4 \times 10^{-7}$ (Table S2) as expected for well-formed SLBs.[34]

Characterization of Supported Lipid Bilayers. The ζ-potentials of SiO_2 sensors and SLBs were determined as previously reported.[69] Briefly, SUVs composed of DOPC alone or a combination of DOPC and DOPG were prepared by mixing the desired ratio of lipids in chloroform, evaporating the solvent with nitrogen gas and additionally under vacuum for 4 h, and hydrating in pH 4 saline (0.01 M NaCl, 0.005 M $CaCl_2$, adjusted to pH 4 with 0.1 M HCl). The mixtures were extruded at least 31 times through a 0.05 μm polycarbonate membrane (Whatman Ltd., UK), stored at 4 °C and used within 10 days of preparation. Silicon wafers with a thermal oxide layer of 30 nm were used as solid supports. The substrates were cleaned in an aqueous solution of NH_4OH and H_2O_2, 1:1 v/v, at 70 °C for 10 min and rinsed intensively with ultrapure water. Prior to the preparation of supported lipid bilayers, the substrates were treated in a plasma chamber at high RF for 2 min to render the surface hydrophilic (Harrick Plasma, Ithaca, USA). Subsequently the measuring cells were assembled, and the lipid vesicle suspensions (0.2 mg mL^{-1} in 0.001 M KCl solution) were injected into the cells and incubated for 2 h at 22 °C. After incubation, the cells were excessively rinsed 10 times with the electrolyte used for the subsequent streaming current measurements. Streaming current measurements were preformed using the Microslit Electrokinetic Setup.[69] ζ-potentials were calculated from steaming current data using the Smoluchowski equation.[74]

Atomic Force Microscopy (AFM). We imaged supported lipid bilayers before and after introduction of DNPs by AFM to determine the surface coverage of PAH-DNPs on the bilayer surfaces. SLBs were formed on ultraflat thermal SiO_2 wafers (Ted Pella) following the procedure described above for QCM-D measurements. All images were collected in tapping mode (1 Hz scan rate) using a Multimode™ atomic force microscope (Bruker). Further details are provided in Text S2.

Results and Discussion

Nanoparticle Hydrodynamic and Electrokinetic Properties. We determined the hydrodynamic diameters and ζ-potentials of the diamond nanoparticles in ultrapure water and in solutions buffered to pH 7.4 with 0.01 M Tris and ionic strength adjusted with NaCl. As-received DNPs had d_h of 16 ± 1.4 nm and ζ-potentials of –35 ± 1 mV in ultrapure water. Wrapping the DNPs with PAH led to changes in their hydrodynamic and electrokinetic properties (Figure 1). PAH-DNPs had d_h of 23 ± 2 nm in ultrapure water, and 28 ± 1 nm, 29 ± 1 nm, and 27 ± 1 nm at ionic strengths of 0.006, 0.016, and 0.106 M, respectively. The relatively invariant hydrodynamic diameter of the PAH-DNPs enabled study of their attachment to SLBs at different salt concentrations without concomitant effects of particles aggregation. The positive ζ-potential of PAH-DNPs decreased with increasing ionic strength (45 ± 1, 43 ±1, and 34 ±5 mV at ionic strengths of 0.006, 0.016, and 0.106 M), consistent with charge screening by the electrolyte.

Electrokinetic Properties of Silica-Supported Lipid Bilayers. We determined ζ-potentials of the SiO_2

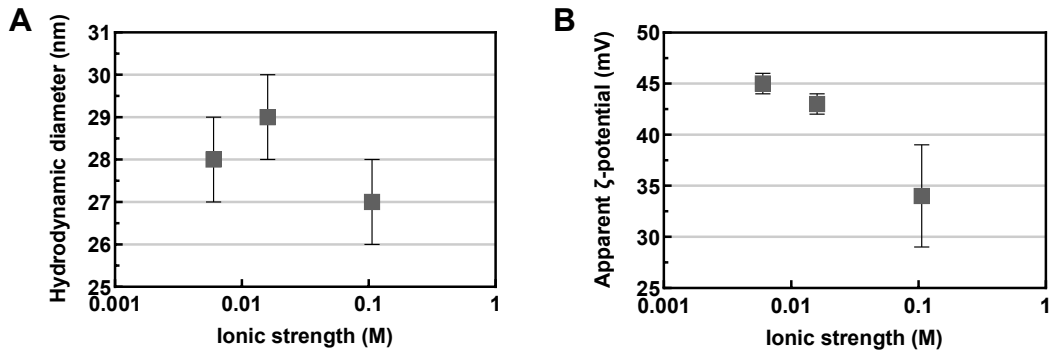

Figure 1. (A) Number-average hydrodynamic diameters and (B) ζ-potential of poly(allylamine HCl)-wrapped diamond nanoparticles (PAH-DNPs) as a function of solution ionic strength. Solutions were buffered to pH 7.4 with 0.01 M Tris and ionic strength adjusted with NaCl. Data points represent the mean of six replicates. Error bars denote one standard deviation. Numerical data are tabulated in Table S2.

substrates and silica-supported lipid bilayers in 0.01 M NaCl (buffered to pH 7.4 with 0.01 M Tris) from streaming current measurements (Figure S2). The silica substrates exhibited a large negative ζ-potential (−81 ± 4 mV), which is not significantly different ($p > 0.05$) than what we found for 0.01 M KCl (-75.6 ± 2.1 mV) at pH 7.5 in the absence of Tris. Supported lipid bilayers composed of the zwitterionic phospholipid DOPC exhibited a negative ζ-potential (−11.3 ± 0.8 mV), slightly more negative than that obtained for the corresponding vesicles under the same solution conditions (–5 ± 1 mV), likely reflecting the influence of the underlying silica substrate on the ζ-potential of the adlayer. The ζ-potential measured here was slightly less negative than that reported previously for SiO_2-supported DOPC bilayers in the absence of Tris and in 0.01 M KCl (−17.5 ± 0.7 mV, pH 7.5).[69] The difference is attributed to the presence of Tris cations,[33] as the isoelectric point of DOPC bilayers in the presence of Na^+ or K^+ is indistinguishable.[75] Incorporation of 10 mass% DOPG to DOPC bilayers decreased the ζ-potential to −57.0 ± 2.3 mV. While these SLBs were formed from SUVs containing 10% DOPG, we expect some degree of asymmetry in the distribution of the anionic phospholipid between the two leaflets of the bilayer due to electrostatic repulsion between the SiO_2 surface and the anionic DOPG leading to enrichment of the anionic lipid in the distal leaflet.[76–78]

Attachment of PAH-DNP to Silica-Coated QCM-D Sensor. We investigated the attachment of PAH-DNPs to SiO_2-coated substrates under the same conditions used to study their interaction with bilayers (*vide infra*). The final acoustic surface mass densities (Γ_{QCM-D}) attained by nanoparticles on silica substrates (Figure 2A) increased with increasing salt concentration. We attribute this trend to charge screening by the electrolyte reducing the electrostatic repulsion between adjacent PAH-DNPs on the silica surface. Electrostatic repulsion between adjacent particles is largest at the lowest ionic strength, leading to a lower surface coverage than at higher ionic strength. The extent of adsorption increases with decreasing adsorbate charge density or as the Debye screening length decreases and interactions between particles occur over shorter distance. This behavior has been commonly reported for adsorption of polyelectrolytes on solid surfaces.[79–81]

Random sequential adsorption (RSA) modeling[82] was used to estimate the jamming limit of particles packing onto the silica substrate. Details are provided in Text S3. The jamming limit predicted by RSA was 7733 $ng \cdot cm^{-2}$, corresponding to a fractional surface coverage of 0.547 and $\Delta f_v/n$ = 430 Hz.[81] Based on this estimate,

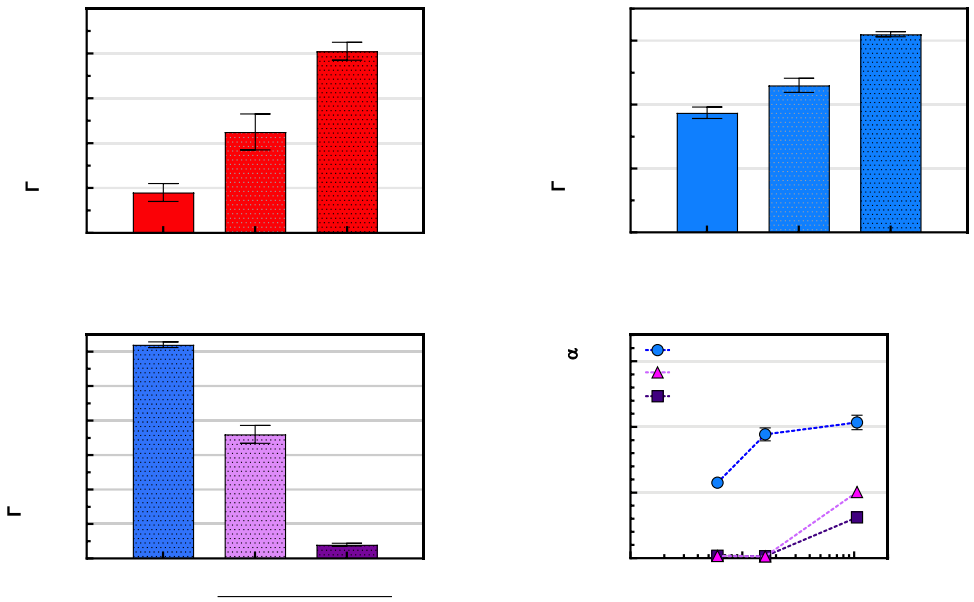

Figure 2. Final surface mass densities (Γ_{QCM-D}) attained by PAH-DNPs on (A) SiO_2 substrates. (B) supported DOPC bilayers ($p \leq 0.0001$), and (C) supported DOPC bilayers containing the indicated amount of DOPG at I = 0.106 M ($p < 0.05$). (D) Attachment efficiencies (α_d) for PAH-DNP attachment to indicated supported lipid bilayers; two-way ANOVA with Tukey's multiple comparisons test (Prism 6.0) was used for statistical analysis. Bars correspond to mean values. Error bars indicate one standard deviation ($n \geq 3$); in some cases, error bars are smaller than symbols. Numerical data are presented inTable S4 and S5. Representative QCM-D traces of PAH-DNP attachment to SiO2 are illustrated in Figure S3.

the PAH-DNP attachment to the silica substrate we observe is well below the jamming limit, displaying fractional coverages of 0.01, 0.03, and 0.06 at ionic strength values of 0.006, 0.016, and 0.106 M, respectively. The Debye screening length ranges from 2.4 nm to 0.93 nm over this concentration range and is always smaller than diameter of the PAH-DNPs, indicating that unfavorable electrostatic nanoparticle-nanoparticle interactions are not limiting packing. On the other hand, the attachment traces suggested that PAH-DNPs attained the maximum surface coverage quickly (Figure S3); rapid drops in frequency (up to 4 Hz in less than 1 min) followed by leveling to steady values. This behavior prompted us to investigate the influence of unbound PAH in the PAH-DNP suspension on nanoparticle adsorption onto the SiO_2 surface. Results for attachment of PAH alone (no DNPs) on silica are presented in Table S4. The extent of final attachment for unbound PAH on silica was comparable to that value for PAH-DNPs (Table S5), indicating that unbound PAH in the PAH-DNP suspension was responsible for some portion of the acoustic mass attained during the adsorption process.[49] At early timepoints, adsorption is diffusion-limited. The diffusivity of free PAH is higher than that of PAH-DNPs, leading to the free PAH commencing attachment to the SiO_2 surface prior to PAH-DNPs. Later in time during the adsorption process, as PAH-DNPs approach the sensor surface, they encounter a PAH-coated surface leading to a decrease in adsorption rate due to an electrostatic barrier. As a result, $\Delta f_n/n$ plateaus, reflecting a pseudo-steady-state condition. These results show that the different *dynamics* of adsorption of free PAH and of PAH-coating DNPS leads to a final surface coverage far below what was expected from RSA. In fact, if we assume that the maximal amount of PAH is adsorbed to the SiO_2 surface, then the acoustic mass attributable to PAH-DNPs and dynamically coupled solvent on the silica substrate would be $\leq$ 2 ng·cm^{-2}. Our results demonstrate that excess molecules in solution, including non-covalently grafted coatings and excess ligand, can significantly impact the attachment of NPs to surfaces. These results further prompted us to explicitly investigate the influence of free PAH on the interaction of PAH-DNP with supported phospholipid bilayers.

Influence of Unbound PAH on Attachment of PAH-DNP to Supported Lipid Bilayers. The results of QCM-D measurements for attachment of free PAH polymer (no DNPs) to supported lipid bilayers showed that PAH bound to all bilayers studied (Table S4). Changes in Γ_{QCM-D} due to the adsorption of free PAH to lipid bilayers were far below those observed with PAH-DNPs (Table S5); furthermore, the extent of PAH attachment increased as the DOPG content of the bilayer increased (Figure 3A); this trend is opposite of what was observed with PAH-DNPs. At I = 0.106 M, Γ_{QCM-D} due to the adsorption of free PAH were 72 ± 6 ng·cm^{-2}, 82 ± 8 ng·cm^{-2}, and 91 ± 15 ng·cm^{-2} on pure DOPC, DOPC + 10% DOPG and DOPC + 20% DOPG, respectively (Table S4). We attribute this trend to stronger electrostatic attraction between the cationic polyelectrolyte and more negatively charged supported lipid bilayers. The final acoustic surface mass density attained by PAH was only 2.3% of that attained by PAH-DNPs on pure DOPC bilayer, 4.5% of that attained by PAH-DNPs on DOPC+10% DOPG, and 45% of that attained by PAH-

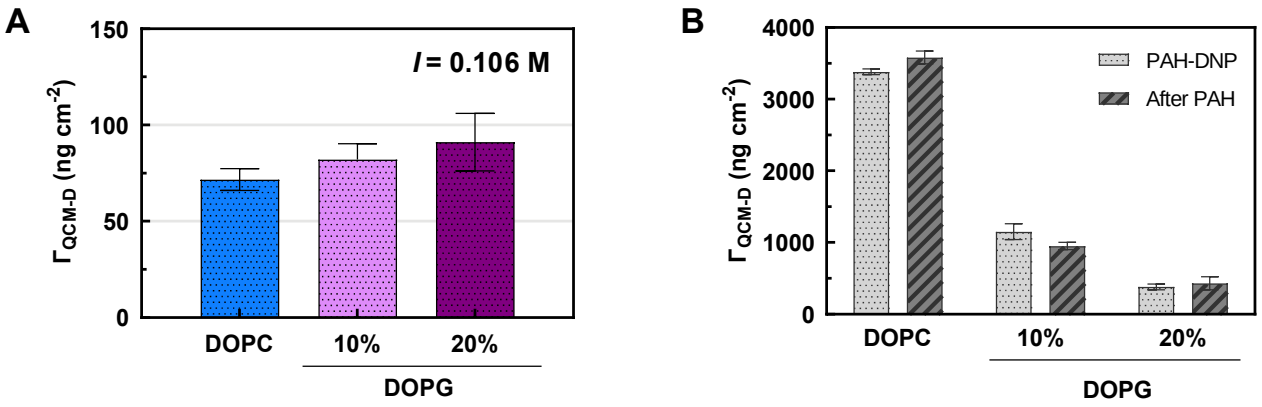

Figure 3. (A) Poly(allylamine hydrochloride) adsorption to supported DOPC bilayers containing 0, 10, or 20% DOPG ($p < 0.05$). (B) Influence of adsorbed PAH polymer on subsequent attachment of PAH-DNPs to supported phospholipid bilayers. In (B), after 50 mg·L-1 PAH polymer had attained maximal adsorption to the surface, PAH-DNPs were introduced to the QCM-D flow cell. Experiments were conducted at I = 0.106 M and pH 7.4 (0.01 M Tris). Bars correspond to mean values; error bars indicate one standard deviation (n = 3).

DNPs on DOPC+20%DOPG. These results imply that free PAH had more impact on PAH-DNP attachment to SLBs as the DOPG content of the bilayer increased.

To probe whether free PAH caused the decrease in maximal attachment of PAH-DNPs as DOPG content in the DOPC bilayer increased (Figure 2C), we conducted experiments in which PAH-DNPs were introduced to QCM-D flow cells after PAH polymer (50 $mg \cdot L^{-1}$) had attained maximal adsorption on the surface (Figure S4). For DOPC + 10% DOPG bilayers after free PAH polymer had attained maximal attachment, overall PAH-DNP attachment saw only a minute decrease (p=0.0025) and no significant decrease in total attachment was observed in DOPC + 20% DOPG bilayers (Figure 3B). Given these results, we do not attribute the decrease in PAH-DNP attachment to DOPC bilayers containing increasing amounts of DOPG to free PAH attachment. Previous studies have also shown that PAH attachment to SLBs is reversible and non-disruptive under our experimental conditions[52]

It should be noted that although PAH-DNPs demonstrated only a small decrease in overall attachment to a DOPC + 10% DOPG bilayer exposed to free PAH, there was a significant decline in initial attachment rate compared to unexposed bilayers; at I = 0.106 M, $(df_5/dt)_{initial}$ of PAH-DNP to the virgin bilayer over the first 30 s was 0.269 ± 0.068 $Hz \cdot s^{-1}$ compared to 0.034 ± 0.003 $Hz \cdot s^{-1}$ for PAH-DNP on bilayers exposed to free PAH. Further, adsorption of PAH-DNP to a virgin DOPC + 10% DOPG bilayer over the first 30 s was comparable to that for free PAH; at I = 0.106 M, $(df_5/dt)_{initial}$ were 0.270 ± 0.003 $Hz \cdot s^{-1}$ for free PAH polymer and 0.269 ± 0.068 $Hz \cdot s^{-1}$ for PAH-DNP. This result implies that free PAH, in equilibrium with bound PAH in nanoparticle solution, was responsible for the change in frequency over the first 30 s of attachment. The diffusivity of free PAH is higher than that of PAH-DNPs, leading to the free PAH attachment to the bilayer surface prior to PAH-DNPs. Based on this result, initial attachment rates (r_d) for PAH-DNP were defined as $d\Gamma_{QCM\text{-}D}/dt$ over the second 30 s of attachment (i.e., t = 30 to 60 s) (Figure S6).

Attachment of PAH-DNP to Supported Zwitterionic DOPC Bilayers. Attachment efficiencies (α_d) for PAH-DNP attachment to supported DOPC bilayers increased with increasing ionic strength (Figure 2D and Table S6), consistent with charge screening reducing the electrostatic repulsion between the PAH-DNP and free PAH adsorbed on the supported DOPC bilayer. The final acoustic mass densities resulting from interaction of PAH-DNPs with DOPC bilayers also increased with increasing ionic strength (Figure 2B and Table S5), as was the case for attachment to SiO_2.[82]Rinsing the bilayers with nanoparticle-free solution of otherwise identical composition produced an increase in frequency of ~1 Hz, indicating that PAH-DNP attachment to DOPC bilayers was largely irreversible on the timescales and under the conditions of the experiments.

Attachment of PAH-DNPs to the negatively charged SiO_2 substrate occurred under electrostatically more favorable conditions relative to attachment to the DOPC bilayers. Despite this, $\Gamma_{QCM\text{-}D}$ for PAH-DNP attachment to DOPC bilayers far exceeded that to the SiO_2 substrates (Table S5). These results suggest that PAH-DNP attachment to SiO_2 substrates and DOPC bilayers occur through different mechanisms. We hypothesize that similar to the SiO_2 surface, the lateral electrostatic repulsion between PAH-DNPs on the DOPC bilayer surface ultimately determines the extent of NPs attachment. The higher packing density of PAH-DNP on the DOPC bilayer suggests that lateral repulsion between diamond nanoparticles is diminished on the lipid bilayer compared to the silica surface. We previously reported that the effective charge density of PAH-wrapped gold nanoparticles is reduced when they attach to the 9:1 DOPC:DOTAP lipid bilayer.[33] Upon attachment, interaction with the negatively charged phosphate groups in the phosphatidylcholine headgroups, and/or any negatively charged counterions associated with the electrical double layer above them, reduces the net charge of the attached particles. The reduction in repulsion between PAH-DNP particles on the DOPC bilayer may result from the recruitment of phospholipid molecules to the nanoparticle surface, reducing the effective charge density of the (now) lipid-coated particles. Formation of a phospholipid corona on nanoparticles wrapped in cationic polyelectrolytes has been previously reported.[83,84] Computational analysis of ions and lipid distributions around the nanoparticle indicated that the cationic PAH polymer plays the key role of attracting lipids by contact ion pairing between the ammonium groups on the polymer and phosphate and glycerol groups on the lipid.[83]

Attachment of PAH-DNP to Supported DOPC Bilayers Containing Anionic DOPG. We next investigated the effect of the incorporation of the anionic phospholipid DOPG into silica-supported DOPC bilayers on the rate and extent of PAH-DNP attachment. The maximum extent of attachment significantly decreased as the DOPG content of SLBs increased from 0 to 20% (Table S4). Results for PAH-DNP attachment to

zwitterionic and anionic SLBs at *I* = 0.106 M are shown in Figure 2C. Although Γ_{QCM-D} for PAH-DNP attachment to bilayers were below the jamming limit (7733 ng·cm^{-2}), they all exceeded that to SiO_2 substrates (81 ± 4 ng·cm^{-2}). Adsorption to bilayers in excess of the maximal extent of attachment to SiO_2 implies a reduction in lateral repulsion between PAH-DNPs on the bilayers, albeit to a lesser degree than on DOPC-only bilayers. Visualization of PAH-DNP attachment to supported DOPC bilayers containing 0%, 10%, or 20% DOPG by AFM showed a qualitatively similar trend (Figure S5). The fractional surface coverage of PAH-DNP as determined by AFM decreased as the DOPG content of the bilayer increased (from 9.2 ± 5.3 for pure DOPC to 5.0 ± 1.9 and 2.3 ± 0.3% for DOPC containing 10% and 20% DOPG, respectively).

We attribute the decrease in maximum attachment with increasing DOPG content in the bilayer to diminishing phospholipid recruitment by the PAH-DNPs leading to decreasing reductions in interparticle repulsion on the surface. The presence of DOPG in the bilayers may increase hydrogen bonding interactions between lipid headgroups, thereby limiting extraction of phospholipids from the bilayer by PAH-DNP and lessening the reduction in interparticle repulsion achieved by acquisition of a lipid corona. Several studies have indicated that incorporation of phospholipids bearing PG headgroups into bilayers composed of PC lipids increases intermolecular headgroup–headgroup interaction relative to the pure PC case.[85–87] Molecular dynamic simulations show that in POPC/POPG bilayers, about 75% of all the POPG lipids are engaged in hydrogen bonding with either POPC or other POPG lipids, while in POPC bilayers, an insignificant number of POPC–POPC hydrogen bonds are detected.[87] Moreover, salt concentrations as low as 0.01 M decrease the lateral diffusion of DOPG in bilayers due to binding of Na^+ or Ca^{2+} to the negative DOPG headgroups, resulting in closer packing of DOPG lipids and thereby increasing bilayer rigidity, an effect not seen with zwitterionic phospholipids.[88] The increase in bilayer rigidity and intermolecular forces between phospholipid headgroups would make lipid extraction more difficult, as these interactions would have to be disrupted in the extraction process. We examine the extent of lipid extraction from DOPC bilayers containing varying amounts of DOPG in the next section.

Attachment efficiencies of PAH-DNPs to SLBs also decreased as the amount of DOPG incorporated into the bilayer increased from 0 to 20% (Figure 2D). This trend held for all ionic strength conditions examined. The trend in attachment efficiencies (α_d) with increasing DOPG content is opposite of that expected from increased electrostatic attraction between the cationic DNPs and the anionic SLB. We attribute this trend to the increased overall adsorption of free PAH polymer to the bilayers with increasing DOPG content (Figure 3A) prior to PAH-DNPs leading to charge neutralization on the bilayer surfaces and reduction of electrostatic attraction between PAH-DNP and supported lipid bilayers, similar to the decrease in attachment rate of PAH-DNPs to DOPC + 10% DOPG bilayers after exposure to free PAH polymer (*vide supra*).

Extraction of Lipids from Supported Lipid Bilayers. Recruitment of phospholipids to the surfaces of PAH-DNP would be expected to alter the electrokinetic properties of the particles. Extraction of lipids by gold NPs from lipid bilayers has been reported previously on the basis of neutron reflectivity

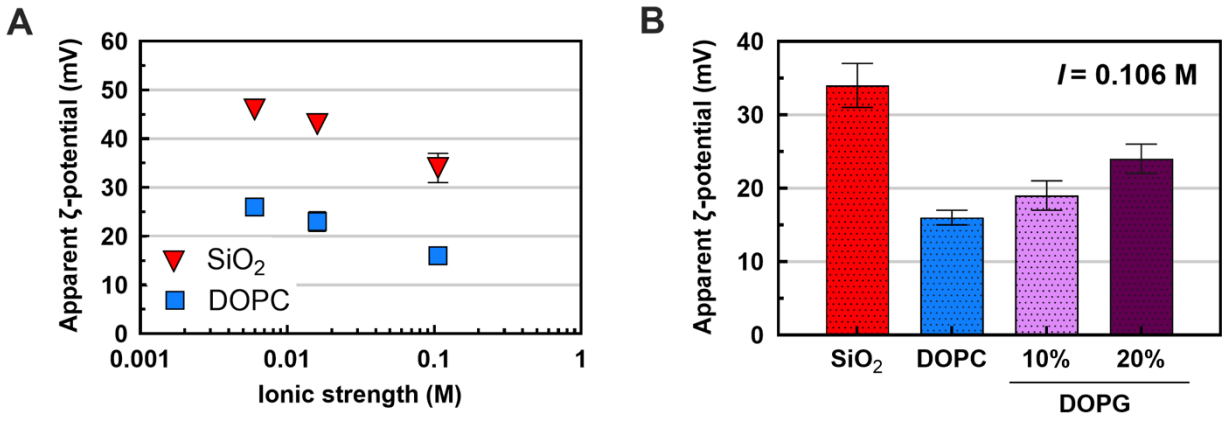

Figure 4. ζ-potentials of PAH-DNP after flowing across (A) bare SiO2 sensors and DOPC bilayers as a function of ionic strength and (B) bare SiO2 sensors and DOPC bilayers containing 0, 10 and 20% DOPG at I = 0.106 M. Data points and bars correspond to mean values; error bars indicate one standard deviation (*n* = 6).

experiments and supported by molecular dynamics simulations.[90] To examine this possibility, we collected PAH-DNPs rinsed from the bilayer and compared their ζ-potentials with those of PAH-DNPs that had passed through a flow cell lacking a bilayer. We found that the ζ-potentials of PAH-DNP rinsed from the DOPC bilayer were lower than those of particles rinsed from the bare SiO_2 substrates (Figure 4A), consistent with them extracting DOPC molecules from the bilayer and acquiring a lipid corona. The reduction in the ζ-potential of the particles due to the acquisition of lipids was roughly the same (~20 mV) over all ionic strengths investigated. The PAH molecules were not covalently bound to the DNPs and one may reasonably question whether the reduction in ζ-potential was not due rather to loss of PAH molecules from the DNPs that were rinsed from the bilayer. We consider this possibility less likely than the particles acquiring a lipid corona. First, the ζ-potentials of the PAH-DNPs exiting the flow cell containing the bare SiO_2-coated QCM-D sensor did not differ from those measured prior to the experiments ($p > 0.05$; compare Figures 1B and 4). This would imply no discernable loss of PAH from the DNPs that had been in contact with the SiO_2 surface. Second, the detachment rate of PAH-DNPs from the silica substrate was less than those from the bilayers. At I = 0.106 M, PAH-DNPs detachment rates were 0.022 ± 0.006 Hz·min^{-1}, 0.067 ± 0.023 Hz·min^{-1}, 0.077 ± 0.028 Hz·min^{-1}, and 0.091 ± 0.030 Hz·min^{-1} from SiO_2, pure DOPC, DOPC + 10% DOPG, and DOPC + 20% DOPG, respectively. This implies stronger interaction with the SiO_2 surface than to the bilayers and therefore a higher likelihood of PAH detachment from the particles.

To test the hypothesis that incorporation of DOPG into DOPC bilayers reduces lipid extraction by the PAH-DNP, we collected particles rinsed from DOPC bilayers containing 0, 10, and 20% DOPG and determined their ζ-potentials (Figure 4B). While in all cases, ζ-potentials for PAH-DNP rinsed from the bilayers were lower than those rinsed from the bare SiO_2 substrates, the degree of reduction in ζ-potential declined as the DOPG content of the bilayers increased. This trend is attributed to lipid extraction decreasing as the anionic DOPG phospholipid content in the bilayers increased. With zwitterionic DOPC bilayers, PAH-DNP would interact with the phosphate group.[83] Accessing the phosphate group of the DOPC headgroup requires tilting of the cationic trimethylamine group away from the like-charged PAH amine and concomitant movement of the phospholipid molecule perpendicular to the plane of the bilayer.[89] This process would disturb hydrophobic interactions and represent a first step in extraction of lipids from the bilayer. In systems with DOPG present, PAH-DNP would also engage in hydrogen bonding with the DOPG head group glycerol moiety,[83] which is less disruptive and may in fact be a reason that less lipid extraction occurs. Thus, while free PAH behaves similarly on the DOPC and DOPC:DOPG bilayers, the PAH-DNPs induce significantly greater bilayer disruption on pure DOPC bilayers due to the ability to extract lipids more effectively from this composition.

Conclusions

We employed quartz crystal microbalance with dissipation monitoring (QCM-D), atomic force microscopy (AFM), and ζ-potential measurements to examine the interactions between PAH-DNPs and supported lipid bilayers composed of either pure DOPC or a mixture of DOPC and DOPG. Our results indicate that in all cases electrostatic attractions between the bilayer and PAH-DNP were responsible for the initial adsorption of particles and lateral electrostatic repulsion between adsorbed particles on the bilayer determined the final extent of PAH-DNP attachment. Adsorption of free PAH, in equilibrium with bound PAH in nanoparticle solution, prior to PAH-DNPs led to a decrease in attachment efficiencies of PAH-DNP to the bilayer and had more impact on PAH-DNP adsorption as the anionic DOPG phospholipid content of the bilayers increased, as more free PAH was adsorbing to the increasingly anionic bilayer. The fractional surface coverage acquired by particles on the DOPC bilayers suggested that mutual repulsion between PAH-DNPs was diminished on the bilayer relative to that attained on SiO_2. We previously showed that the effective charge density of PAH-wrapped gold nanoparticles is reduced when they attach to the DOPC:DOTAP lipid bilayer. Upon attachment, interaction with the negatively charged phosphate groups in the PC headgroups, and/or any negatively charged counterions associated with the electrical double layer above them, reduces the net charge of the adsorbed particles. We further demonstrate that PAH-DNPs extract phospholipid molecules from the DOPC bilayer and acquire a lipid corona. Lipid corona formation on the nanoparticle surface alters the electrokinetic properties of the particles (decreases electrophoretic mobility) and increases the maximum surface mass density attained by the PAH-DNP on the bilayer surface. Incorporation of the anionic phospholipid DOPG into the DOPC bilayers led to an increase in initial adsorption rate but a

decrease in final extent of PAH-DNP attachment to the bilayer. The reduction in final extent of PAH-DNP attachment with increasing DOPG content of the bilayer is attributed to the increase in hydrogen bonding interactions between lipid headgroups that limits extraction of phospholipids from the bilayer by PAH-DNP, lessening the reduction in interparticle repulsion achieved by acquisition of a lipid corona.

This works aids in understanding nanomaterial–phospholipid interactions and may be used to help predict the cytotoxicity of polymer-functionalized nanoparticles. The observation of lipid extraction would likely affect the cell function and could induce toxicity. Recent work assessing PAH-AuNP toxicity to both *Daphnia magna*[91] and *Shewanella oneidensis*[53] shows that particles functionalized with this polymer are toxic to both species, although the mechanism of toxicity was not determined. This study will serve as a baseline for investigating the interactions of polymer-functionalized nanoparticle with biological membranes as well as for comparison with future studies with increasingly complex bilayers or particles that have been altered by the environment or biological media.

Corresponding Author

*Phone: +1 (608) 262-6371; e-mail: rjhamers@wisc.edu

ORCID

Nasim Ganji: 0000-0001-6420-908X
Caroline Anastasia: 0000-0001-7478-5574
Eric S. Melby: 0000-0002-3812-2965
Arielle C. Mensch: 0000-0002-4063-5882
Emily R. Caudill: 0000-0002-3645-9804
Ralf Zimmermann: 0000-0002-6280-3218
Robert J. Hamers: 0000-0003-3821-9625
Joel A. Pedersen: 0000-0002-3918-18660

Conflicts of interest

There are no conflicts to declare.

Acknowledgements

This work was supported by National Science Foundation under the NSF Center for Sustainable Nanotechnology, CHE - 2001611. The NSF CSN is part of the Centers for Chemical Innovation Program.

1 A. M. Farnoud and S. Nazemidashtarjandi, Emerging investigator series: interactions of engineered nanomaterials with the cell plasma membrane; what have we learned from membrane models?, *Environ Sci Nano*, 2019, **6**, 13–40.

2 R. J. Hamers, Nanomaterials and global sustainability, *Acc Chem Res*, 2017, **50**, 633–637.

3 A. Rahnamoun, K. Kim, J. A. Pedersen and R. Hernandez, Ionic Environment Affects Bacterial Lipopolysaccharide Packing and Function, *Langmuir*, 2020, **36**, 3149–3158.

4 A. C. Mensch, E. S. Melby, E. D. Laudadio, I. U. Foreman-Ortiz, Y. Zhang, A. Dohnalkova, D. Hu, J. A. Pedersen, R. J. Hamers and G. Orr, Preferential interactions of primary amine-terminated quantum dots with membrane domain boundaries and lipid rafts revealed with nanometer resolution, *Environ Sci Nano*, 2020, **7**, 149–161.

5 M. Bundschuh, J. Filser, S. Lüderwald, M. S. McKee, G. Metreveli, G. E. Schaumann, R. Schulz and S. Wagner, Nanoparticles in the environment: where do we come from, where do we go to?, *Environ Sci Eur*, 2018, **30**, 1–17.

6 B. Nowack and T. D. Bucheli, *Environmental Pollution*, 2007, 150, 5–22.

7 E. Guzmán and E. Santini, Lung surfactant-particles at fluid interfaces for toxicity assessments, *Curr Opin Colloid Interface Sci*, 2019, **39**, 24–39.

8 A. E. Nel, L. Mädler, D. Velegol, T. Xia, E. M. V Hoek, P. Somasundaran, F. Klaessig, V. Castranova and M. Thompson, Understanding biophysicochemical interactions at the nano-bio interface, *Nat Mater*, 2009, **8**, 543–557.

9 T. Yu, A. Malugin and H. Ghandehari, Impact of silica nanoparticle design on cellular toxicity and hemolytic activity, *ACS Nano*, 2011, **5**, 5717–5728.

10 L. Lai, S. J. Li, J. Feng, P. Mei, Z. H. Ren, Y. L. Chang and Y. Liu, Effects of Surface Charges on

the Bactericide Activity of CdTe/ZnS Quantum Dots: A Cell Membrane Disruption Perspective, *Langmuir*, 2017, **33**, 2378–2386.

11 S. Kang, M. Pinault, L. D. Pfefferle and M. Elimelech, Single-walled carbon nanotubes exhibit strong antimicrobial activity, *Langmuir*, 2007, **23**, 8670–8673.

12 S. Kang, M. Herzberg, D. F. Rodrigues and M. Elimelech, Antibacterial effects of carbon nanotubes: Size does matter!, *Langmuir*, 2008, **24**, 6409–6413.

13 K. L. Chen and G. D. Bothun, Nanoparticles Meet Cell Membranes: Probing Nonspecific Interactions using Model Membranes, *Environ Sci Technol*, 2014, **48**, 873–880.

14 A. K. Sachan, R. K. Harishchandra, C. Bantz, M. Maskos, R. Reichelt and H. J. Galla, High-resolution investigation of nanoparticle interaction with a model pulmonary surfactant monolayer, *ACS Nano*, 2012, **6**, 1677–1687.

15 R. K. Harishchandra, A. K. Sachan, A. Kerth, G. Lentzen, T. Neuhaus and H. J. Galla, Compatible solutes: Ectoine and hydroxyectoine improve functional nanostructures in artificial lung surfactants, *Biochim Biophys Acta Biomembr*, 2011, **1808**, 2830–2840.

16 S. Nazemidashtarjandi and A. M. Farnoud, Membrane outer leaflet is the primary regulator of membrane damage induced by silica nanoparticles in vesicles and erythrocytes, *Environ Sci Nano*, 2019, **6**, 1219–1232.

17 Y. Chen and G. D. Bothun, Lipid-Assisted formation and dispersion of aqueous and bilayer-embedded Nano-C_{60}, *Langmuir*, 2009, **25**, 4875–4879.

18 A. Xi and G. D. Bothun, Centrifugation-based assay for examining nanoparticle-lipid membrane binding and disruption., *Analyst*, 2014, **139**, 973–81.

19 N. Ganji, I. A. Khan and G. D. Bothun, Surface Activity of Poly(ethylene glycol)-Coated Silver Nanoparticles in the Presence of a Lipid Monolayer, *Langmuir*, 2018, **34**, 2039–2045.

20 N. M. Anaya, F. Faghihzadeh, N. Ganji, G. Bothun and V. Oyanedel-craver, Science of the Total Environment Comparative study between chemostat and batch reactors to quantify membrane permeability changes on bacteria exposed to silver nanoparticles, 2016, **565**, 841–848.

21 G. D. Bothun, N. Ganji, I. A. Khan, A. Xi and C. Bobba, Anionic and Cationic Silver Nanoparticle Binding Restructures Net-Anionic PC/PG Monolayers with Saturated or Unsaturated Lipids, *Langmuir*, 2017, **33**, 353–360.

22 E. Guzmán, M. Ferrari, E. Santini, L. Liggieri and F. Ravera, Effect of silica nanoparticles on the interfacial properties of a canonical lipid mixture, *Colloids Surf B Biointerfaces*, 2015, **136**, 971–980.

23 E. Guzmán, L. Liggieri, E. Santini, M. Ferrari and F. Ravera, DPPC-DOPC Langmuir monolayers modified by hydrophilic silica nanoparticles: Phase behaviour, structure and rheology, *Colloids Surf A Physicochem Eng Asp*, 2012, **413**, 174–183.

24 E. S. Melby, A. C. Mensch, S. E. Lohse, D. Hu, G. Orr, C. J. Murphy, R. J. Hamers and J. a. Pedersen, Formation of supported lipid bilayers containing phase-segregated domains and their interaction with gold nanoparticles, *Environ Sci Nano*, 2016, **3**, 45–55.

25 S. Morandat, S. Azouzi, E. Beauvais, A. Mastouri and K. El Kirat, Atomic force microscopy of model lipid membranes, *Anal Bioanal Chem*, 2013, **405**, 1445–1461.

26 E. S. Melby, S. E. Lohse, J. E. Park, A. M. Vartanian, R. A. Putans, H. B. Abbott, R. J. Hamers, C. J. Murphy and J. A. Pedersen,

Cascading Effects of Nanoparticle Coatings: Surface Functionalization Dictates the Assemblage of Complexed Proteins and Subsequent Interaction with Model Cell Membranes, *ACS Nano*, 2017, **11**, 5489–5499.

27 P. Yi and K. L. Chen, Interaction of multiwalled carbon nanotubes with supported lipid bilayers and vesicles as model biological membranes, *Environ Sci Technol*, 2013, **47**, 5711–5719.

28 C. Corredor, W.-C. Hou, S. A. Klein, B. Y. Moghadam, M. Goryll, K. Doudrick, P. Westerhoff and J. D. Posner, Disruption of Model Cell Membranes by Carbon Nanotubes Charlie, *Carbon N Y*, 2013, **60**, 67–75.

29 X. Zhang and S. Yang, Nonspecific adsorption of charged quantum dots on supported zwitterionic lipid bilayers: Real-time monitoring by quartz crystal microbalance with dissipation, *Langmuir*, 2011, **27**, 2528–2535.

30 X. Xiao, G. A. Montaño, T. L. Edwards, A. Allen, K. E. Achyuthan, R. Polsky, D. R. Wheeler and S. M. Brozik, Surface charge dependent nanoparticle disruption and deposition of lipid bilayer assemblies, *Langmuir*, 2012, **28**, 17396–17403.

31 A. C. Mensch, J. T. Buchman, C. L. Haynes, J. A. Pedersen and R. J. Hamers, Quaternary Amine-Terminated Quantum Dots Induce Structural Changes to Supported Lipid Bilayers, *Langmuir*, 2018, **34**, 12369–12378.

32 K. Kim, S. J. Jeon, P. Hu, C. M. Anastasia, W. F. Beimers, J. P. Giraldo and J. A. Pedersen, Sulfolipid density dictates the extent of carbon nanodot interaction with chloroplast membranes, *Environ Sci Nano*, 2022, **9**, 2691–2703.

33 J. M. Troiano, L. L. Olenick, T. R. Kuech, E. S. Melby, D. Hu, S. E. Lohse, A. C. Mensch, M. Dogangun, A. M. Vartanian, M. D. Torelli, E. Ehimiaghe, S. R. Walter, L. Fu, C. R. Anderton, Z. Zhu, H. Wang, G. Orr, C. J. Murphy, R. J. Hamers, J. A. Pedersen and F. M. Geiger, Direct Probes of 4 nm Diameter Gold Nanoparticles Interacting with Supported Lipid Bilayers, *The Journal of Physical Chemistry C*, 2015, **119**, 534–546.

34 N. J. Cho, C. W. Frank, B. Kasemo and F. Höök, Quartz crystal microbalance with dissipation monitoring of supported lipid bilayers on various substrates, *Nat Protoc*, 2010, **5**, 1096–1106.

35 E. S. Melby, S. E. Lohse, J. E. Park, A. M. Vartanian, R. A. Putans, H. B. Abbott, R. J. Hamers, C. J. Murphy and J. A. Pedersen, Cascading Effects of Nanoparticle Coatings: Surface Functionalization Dictates the Assemblage of Complexed Proteins and Subsequent Interaction with Model Cell Membranes, *ACS Nano*, 2017, **11**, 5489–5499.

36 P. R. Leroueil, S. A. Berry, K. Duthie, G. Han, V. M. Rotello, D. Q. McNerny, J. R. Baker, B. G. Orr and M. M. B. Holl, Wide varieties of cationic nanoparticles induce defects in supported lipid bilayers, *Nano Lett*, 2008, **8**, 420–424.

37 E. Guzmán, L. Liggieri, E. Santini, M. Ferrari and F. Ravera, Influence of silica nanoparticles on phase behavior and structural properties of DPPC-Palmitic acid Langmuir monolayers, *Soft Matter*, 2012, **8**, 3938–3948.

38 D. Di, M. Maccarini, R. Parker, A. Mackie, G. Fragneto and F. Baldelli, The effect of the protein corona on the interaction between nanoparticles and lipid bilayers, *J Colloid Interface Sci*, 2017, **504**, 741–750.

39 A. Lesniak, A. Salvati, M. J. Santos-Martinez, M. W. Radomski, K. A. Dawson and C. Åberg, Nanoparticle adhesion to the cell membrane and its effect on nanoparticle uptake efficiency, *J Am Chem Soc*, 2013, **135**, 1438–1444.

40 E. Froohlich, The role of surface charge in cellular uptake and cytotoxicity of medical

nanoparticles, *Int J Nanomedicine*, 2012, **7**, 5577–5591.

41 K. H. Jacobson, I. L. Gunsolus, T. R. Kuech, J. M. Troiano, E. S. Melby, S. E. Lohse, D. Hu, W. B. Chrisler, C. J. Murphy, G. Orr, F. M. Geiger, C. L. Haynes and J. A. Pedersen, Lipopolysaccharide Density and Structure Govern the Extent and Distance of Nanoparticle Interaction with Actual and Model Bacterial Outer Membranes, *Environ Sci Technol*, 2015, **49**, 10642–10650.

42 J. K. Sheavly, J. A. Pedersen and R. C. Van Lehn, Curvature-driven adsorption of cationic nanoparticles to phase boundaries in multicomponent lipid bilayers, *Nanoscale*, 2019, **11**, 2767–2778.

43 S. Li and N. Malmstadt, Deformation and poration of lipid bilayer membranes by cationic nanoparticles, *Soft Matter*, 2013, **9**, 4969.

44 B. Y. Moghadam, W. C. Hou, C. Corredor, P. Westerhoff and J. D. Posner, Role of nanoparticle surface functionality in the disruption of model cell membranes, *Langmuir*, 2012, **28**, 16318–16326.

45 P. R. Leroueil, S. Hong, A. Mecke, J. R. Baker, B. G. Orr and M. M. Banaszak Holl, Nanoparticle interaction with biological membranes: does nanotechnology present a Janus face?, *Acc Chem Res*, 2007, **40**, 335–42.

46 T. R. Silva, D. Brondani, E. Zapp and I. CruzVieira, Electrochemical Sensor Based on Gold Nanoparticles Stabilized in Poly(Allylamine hydrochloride) for Determination of Vanillin, *Electroanalysis*, 2015, **27**, 465–472.

47 J. T. Buchman, A. Rahnamoun, K. M. Landy, X. Zhang, A. M. Vartanian, L. M. Jacob, C. J. Murphy, R. Hernandez and C. L. Haynes, Using an environmentally-relevant panel of Gram-negative bacteria to assess the toxicity of polyallylamine hydrochloride-wrapped gold nanoparticles, *Environ Sci Nano*, 2018, **5**, 279–288.

48 N. Dalchand, M. Doğangün, P. E. Ohno, E. Ma, A. B. F. Martinson and F. M. Geiger, Perturbation of Hydrogen-Bonding Networks over Supported Lipid Bilayers by Poly(allylamine hydrochloride), *Journal of Physical Chemistry B*, 2019, **123**, 4251–4257.

49 T. A. Qiu, M. D. Torelli, A. M. Vartanian, N. B. Rackstraw, J. T. Buchman, L. M. Jacob, C. J. Murphy, R. J. Hamers and C. L. Haynes, Quantification of Free Polyelectrolytes Present in Colloidal Suspension, Revealing a Source of Toxic Responses for Polyelectrolyte-Wrapped Gold Nanoparticles, *Anal Chem*, 2017, **89**, 1823–1830.

50 A. M. Alkilany, P. K. Nagaria, C. R. Hexel, T. J. Shaw, C. J. Murphy and M. D. Wyatt, Cellular uptake and cytotoxicity of gold nanorods: Molecular origin of cytotoxicity and surface effects, *Small*, 2009, **5**, 701–708.

51 B. Harper, F. Sinche, R. Ho Wu, M. Gowrishankar, G. Marquart, M. Mackiewicz and S. Harper, The Impact of Surface Ligands and Synthesis Method on the Toxicity of Glutathione-Coated Gold Nanoparticles, *Nanomaterials*, 2014, **4**, 355–371.

52 J. M. Troiano, A. C. McGeachy, L. L. Olenick, D. Fang, D. Liang, J. Hong, T. R. Kuech, E. R. Caudill, J. A. Pedersen, Q. Cui and F. M. Geiger, Quantifying the Electrostatics of Polycation-Lipid Bilayer Interactions, *J Am Chem Soc*, 2017, **139**, 5808–5816.

53 Z. V. Feng, I. L. Gunsolus, T. A. Qiu, K. R. Hurley, L. H. Nyberg, H. Frew, K. P. Johnson, A. M. Vartanian, L. M. Jacob, S. E. Lohse, M. D. Torelli, R. J. Hamers, C. J. Murphy and C. L. Haynes, Impacts of gold nanoparticle charge and ligand type on surface binding and toxicity to Gram-

negative and Gram-positive bacteria, *Chem Sci*, 2015, **6**, 5186–5196.

54 T. A. Qiu, J. S. Bozich, S. E. Lohse, A. M. Vartanian, L. M. Jacob, B. M. Meyer, I. L. Gunsolus, N. J. Niemuth, C. J. Murphy, C. L. Haynes and R. D. Klaper, Gene expression as an indicator of the molecular response and toxicity in the bacterium *Shewanella oneidensis* and the water flea *Daphnia magna* exposed to functionalized gold nanoparticles, *Environ Sci Nano*, 2015, **2**, 615–629.

55 G. A. Dominguez, S. E. Lohse, M. D. Torelli, C. J. Murphy, R. J. Hamers, G. Orr and R. D. Klaper, Effects of charge and surface ligand properties of nanoparticles on oxidative stress and gene expression within the gut of Daphnia magna, *Aquatic Toxicology*, 2015, **162**, 1–9.

56 A. C. Mensch, R. T. Hernandez, J. E. Kuether, M. D. Torelli, Z. V. Feng, R. J. Hamers and J. A. Pedersen, Natural Organic Matter Concentration Impacts the Interaction of Functionalized Diamond Nanoparticles with Model and Actual Bacterial Membranes, *Environ Sci Technol*, 2017, **51**, 11075–11084.

57 B. U. Nobbmann, Intensity-Volume-Number: Which size is correct ?, *Technical Note MRK1357-01; Malvern Instruments: Malvern, U.K.*, 2009, 1–5.

58 H. Ohshima, Electrokinetics of soft particles, *Colloid Polym Sci*, 2007, **285**, 1411–1421.

59 M. Rodahl, F. Höök, A. Krozer, P. Brzezinski and B. Kasemo, Quartz crystal microbalance setup for frequency and Q-factor measurements in gaseous and liquid environments, *Review of Scientific Instruments*, 1995, **66**, 3924–3930.

60 C. A. Keller and B. Kasemo, Surface specific kinetics of lipid vesicle adsorption measured with a quartz crystal microbalance, *Biophys J*, 1998, **75**, 1397–1402.

61 I. Reviakine, D. Johannsmann and R. P. Richter, Hearing what you cannot see and visualizing what you hear: Interpreting quartz crystal microbalance data from solvated interfaces, *Anal Chem*, 2011, **83**, 8838–8848.

62 G. Sauerbrey, Verwendung von Schwingquarzen zur Wägung dünner Schichten und zur Mikrowägung, *Zeitschrift für Physik*, 1959, **155**, 206–222.

63 A. Domack, O. Prucker, J. Rühe and D. Johannsmann, Swelling of a polymer brush probed with a quartz crystal resonator, *Phys Rev E*, 1997, **56**, 680–689.

64 M. V Voinova, M. Rodahl, M. Jonson and B. Kasemo, Viscoelastic Acoustic Response of Layered Polymer Films at Fluid-Solid Interfaces: Continuum Mechanics Approach, *Phys Scr*, 1999, **59**, 391–396.

65 N. J. Cho, K. K. Kanazawa, J. S. Glenn and C. W. Frank, Employing two different quartz crystal microbalance models to study changes in viscoelastic behavior upon transformation of lipid vesicles to a bilayer on a gold surface, *Anal Chem*, 2007, **79**, 7027–7035.

66 R. Richter, A. Mukhopadhyay and A. Brisson, Pathways of Lipid Vesicle Deposition on Solid Surfaces: A Combined QCM-D and AFM Study, *Biophys J*, 2003, **85**, 3035–3047.

67 K. L. Chen and M. Elimelech, Aggregation and deposition kinetics of fullerene (C60) nanoparticles, *Langmuir*, 2006, **22**, 10994–11001.

68 Q. Chen, S. Xu, Q. Liu, J. Masliyah and Z. Xu, QCM-D study of nanoparticle interactions, *Adv Colloid Interface Sci*, 2016, **233**, 94–114.

69 R. Zimmermann, D. Küttner, L. Renner, M. Kaufmann, J. Zitzmann, M. Müller and C. Werner, Charging and structure of zwitterionic supported bilayer lipid membranes studied by

streaming current measurements, fluorescence microscopy, and attenuated total reflection Fourier transform infrared spectroscopy, *Biointerphases*, 2009, **4**, 1–6.

70 M. Zhang and M. Akbulut, Adsorption, desorption, and removal of polymeric nanomedicine on and from cellulose surfaces: Effect of size, *Langmuir*, 2011, **27**, 12550–12559.

71 M. Zhang, J. Soto-Rodríguez, I. C. Chen and M. Akbulut, Adsorption and removal dynamics of polymeric micellar nanocarriers loaded with a therapeutic agent on silica surfaces, *Soft Matter*, 2013, **9**, 10155–10164.

72 Y. Zhang, N. V. Hudson-Smith, S. D. Frand, M. S. Cahill, L. S. Davis, Z. V. Feng, C. L. Haynes and R. J. Hamers, Influence of the Spatial Distribution of Cationic Functional Groups at Nanoparticle Surfaces on Bacterial Viability and Membrane Interactions, *J Am Chem Soc*, 2020, **142**, 10814–10823.

73 N. J. Cho, K. K. Kanazawa, J. S. Glenn and C. W. Frank, Employing two different quartz crystal microbalance models to study changes in viscoelastic behavior upon transformation of lipid vesicles to a bilayer on a gold surface, *Anal Chem*, 2007, **79**, 7027–7035.

74 A. Sze, D. Erickson, L. Ren and D. Li, Zeta-potential measurement using the Smoluchowski equation and the slope of the current-time relationship in electroosmotic flow, *J Colloid Interface Sci*, 2003, **261**, 402–410.

75 R. Zimmermann, D. Küttner, L. Renner, M. Kaufmann and C. Werner, Fluidity modulation of phospholipid bilayers by electrolyte ions: Insights from fluorescence microscopy and microslit electrokinetic experiments, *Journal of Physical Chemistry A*, 2012, **116**, 6519–6525.

76 S. Stanglmaier, S. Hertrich, K. Fritz, J. F. Moulin, M. Haese-Seiller, J. O. Rädler and B. Nickel, Asymmetric distribution of anionic phospholipids in supported lipid bilayers, *Langmuir*, 2012, **28**, 10818–10821.

77 H. P. Wacklin, Composition and asymmetry in supported membranes formed by vesicle fusion, *Langmuir*, 2011, **27**, 7698–7707.

78 R. P. Richter, N. Maury and A. R. Brisson, On the effect of the solid support on the interleaflet distribution of lipids in supported lipid bilayers, *Langmuir*, 2005, **21**, 299–304.

79 A. C. McGeachy, N. Dalchand, E. R. Caudill, T. Li, M. Dog, L. L. Olenick, H. Chang, J. A. Pedersen and F. M. Geiger, Interfacial electrostatics of poly(vinylamine hydrochloride), poly(diallyldimethylammonium chloride), poly-L-lysine, and poly-L-arginine interacting with lipid bilayers, *Physical Chemistry Chemical Physics*, 2018, **00**, 1–11.

80 M. A. Cohen Stuart, in *Short and Long Chains at Interfaces*, ed. J. T. T. Van J. Daillant, P. Guenoun, C. Marques. P. Muller, Atlantica Seguier Frontiers, 1995, 1995, pp. 3–12.

81 Z. Adamczyk, L. Szyk and P. Warszyński, Colloid particle adsorption in the slot impinging jet cell, *J Colloid Interface Sci*, 1999, **209**, 350–361.

82 P. Bingen, G. Wang, N. F. Steinmetz, M. Rodahl and R. P. Richter, Solvation effects in the quartz crystal microbalance with dissipation monitoring response to biomolecular adsorption. A phenomenological approach, *Anal Chem*, 2008, **80**, 8880–8890.

83 L. L. Olenick, J. M. Troiano, A. Vartanian, E. S. Melby, A. C. Mensch, L. Zhang, J. Hong, O. Mesele, T. Qiu, J. Bozich, S. Lohse, X. Zhang, T. R. Kuech, A. Millevolte, I. Gunsolus, A. C. McGeachy, M. Doğangün, T. Li, D. Hu, S. R. Walter, A. Mohaimani, A. Schmoldt, M. D. Torelli, K. R. Hurley, J. Dalluge, G. Chong, Z. V. Feng, C. L. Haynes, R. J. Hamers, J. A. Pedersen, Q. Cui, R. Hernandez, R. Klaper, G. Orr, C. J. Murphy and F. M. Geiger, Lipid Corona

Formation from Nanoparticle Interactions with Bilayers, *Chem*, 2018, **4**, 2709–2723.

84 C. A. Lochbaum, A. K. Chew, X. Zhang, V. Rotello, R. C. Van Lehn and J. A. Pedersen, Lipophilicity of Cationic Ligands Promotes Irreversible Adsorption of Nanoparticles to Lipid Bilayers, *ACS Nano*, 2021, **15**, 6562–6572.

85 K. Balali-Mood, T. A. Harroun and J. P. Bradshaw, Molecular dynamics simulations of a mixed DOPC / DOPG bilayer, *European Biophysics Journal*, 2003, **12**, S135–S140.

86 T. Broemstrup and N. Reuter, Molecular dynamics simulations of mixed acidic/zwitterionic phospholipid bilayers, *Biophys J*, 2010, **99**, 825–833.

87 L. Janosi and A. A. Gorfe, Simulating POPC and POPC/POPG bilayers: Conserved packing and altered surface reactivity, *J Chem Theory Comput*, 2010, **6**, 3267–3273.

88 A. Filippov, G. Oradd and G. Lindblom, Effect of NaCl and CaCl2 on the lateral diffusion of zwitterionic and anionic lipids in bilayers, *Chem Phys Lipids*, 2009, **159**, 81–87.

89 B. Wang, L. Zhang, C. B. Sung and S. Granick, Nanoparticle-induced surface reconstruction of phospholipid membranes, *Proc Natl Acad Sci U S A*, 2008, **105**, 18171–18175.

90 F. Lolicato, L. Joly, H. Martinez-Seara, G. Fragneto, E. Scoppola, F. Bombelli, I. Vattulainen, J. Akola, and M. Maccarini, The Role of Temperature and Lipid Charge on Intake/Uptake of Cationic Gold Nanoparticles into Lipid Bilayers, *Small*, 2019, **15**, 1805046.

91 J. S. Bozich, S. E. Lohse, M. D. Torelli, C. J. Murphy, R. J. Hamers and R. D. Klaper, Surface chemistry, charge and ligand type impact the toxicity of gold nanoparticles to *Daphnia magna*, *Environ Sci Nano*, 2014, **1**, 260–270.